# Focusing analysis of the pinhole photon sieve: Individual far-field model

**2 authors**, including:

Jürgen Jahns
FernUniversität in Hagen
**211** PUBLICATIONS **2,839** CITATIONS

Some of the authors of this publication are also working on these related projects:

Project   Planar Optics for Interconnects View project

Project   Microoptical processing and shaping of ultrashort pulses View project

# Focusing analysis of the pinhole photon sieve: individual far-field model

**Qing Cao and Jürgen Jahns**

*Universität Hagen, Optische Nachrichtentechnik, Universitätsstrasse 27/PRG, 58084 Hagen, Germany*

Recently, a new class of diffractive optical element called a photon sieve, which consists of a great number of pinholes, was developed for the focusing and imaging of soft x rays. In terms of the closed-form formula for the far field of individual pinholes and the linear superposition principle, we present a simple yet accurate analytical model for the focusing of the pinhole photon sieve. This model is applicable to arbitrary paraxial illumination with arbitrary complex amplitude distribution at the photon sieve plane. We check the validity range of this model by comparing it with the exact Fresnel diffraction integral. Some special problems, such as the individual quasi-far-field correction for very large pinholes and the related phase shift induced by this correction, are also discussed. © 2002 Optical Society of America

*OCIS codes:* 220.2560, 050.1970, 340.7480, 050.1940, 110.1220, 350.3950.

## 1. INTRODUCTION

The focusing and imaging of soft x rays has many applications in physical and life sciences, such as in high-resolution x-ray microscopy, spectroscopy, and lithography. It is difficult to use a traditional refractive lens to focus soft x rays, because of the strong absorption of solid materials in this spectral region. Fresnel zone plates can be used for this kind of focusing.[1] However, the largest spatial resolution that can be achieved by Fresnel zone plates is directly related to the width of the outermost zone[2,3] and is therefore limited by the smallest structure (20–40 nm) that can be fabricated by lithography.[2] To overcome the limitations of Fresnel zone plates, Kipp *et al.*[3] recently developed a novel diffractive optical element called a photon sieve, which consists of a great number of pinholes properly distributed over the Fresnel zones, for the focusing and imaging of soft x rays. The crucial idea of the photon sieve is that each pinhole has a positive contribution to the field value at the desired focal point. This kind of collective behavior can greatly enhance the intensity at the desired focal point and lead to the focusing. In Ref. 3, the authors employed the traditional Fresnel zone plate theory and the numerical calculation of Fresnel–Kirchhoff diffraction integrals to analyze and design the photon sieve.

In this paper, we shall present a simple yet accurate analytical model for the focusing and imaging of the pinhole photon sieve. This model is based on the far-field formula of individual pinholes and the linear superposition principle and is applicable to arbitrary paraxial illumination with arbitrary complex amplitude distribution at the photon sieve plane. We shall also check the validity range of this model and discuss some related problems such as the individual quasi-far-field correction for very large pinholes. We shall limit our analysis to the performance of the individual pinholes and not discuss the statistical aspects (filtering, apodization, and quasi-random behaviors) of the photon sieve.

## 2. INDIVIDUAL FAR-FIELD MODEL

As shown in Fig. 1, a general photon sieve, which consists of a great number of pinholes whose locations and radii are properly chosen, is located at the $xy$ plane, the desired focal point is located at the point $(X = 0, Y = 0)$, and the distance between the $xy$ plane and the $XY$ plane is $q$. We denote by $V(x, y) = A(x, y)\exp[jkL(x, y)]$ the complex amplitude distribution of the paraxial illumination beam at the photon sieve plane, where $k = 2\pi/\lambda$ is the wave number, $\lambda$ is the wavelength, $j = \sqrt{-1}$ is the imaginary unit, $L(x, y)$ is the eikonal, and $A(x, y)$ is the real amplitude. According to the linear superposition principle, the total diffracted field $U(x, y)$ at the focal plane is the simple sum of those individual diffracted fields from different pinholes. That is to say, $U(X, Y) = \Sigma_{n=1}^{N} U_n(X, Y)$, where $U_n(X, Y)$ is the individual diffracted field from the $n$th pinhole and $N$ is the number of pinholes. Consider the $n$th pinhole, whose central location and radius are denoted by $(x = x_n, y = y_n)$ and $a_n$, respectively. From the Fresnel diffraction integral formula, the corresponding diffracted field $U_n(X, Y)$ can be expressed as

$$
U_n(X, Y) = \frac{1}{\lambda q} \int \int_{-\infty}^{\infty} V_n(x, y)
$$

$$
\times \exp\left[jk \frac{(X - x)^2 + (Y - y)^2}{2q}\right] dx\, dy,
$$

$$(1)$$

where $V_n(x, y) = V(x, y)$ inside the pinhole and $V_n(x, y) = 0$ outside the pinhole. In Eq. (1), we have ignored the common factor $-j \exp(jkq)$ for simplicity. Because the change of the field inside the pinhole is very small, the complex amplitude distribution inside the pinhole can be expressed as the local plane wave
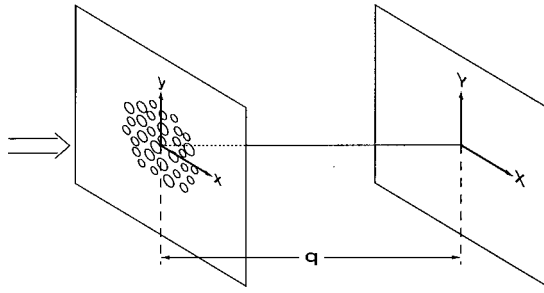
Fig. 1. Schematic view of a general photon sieve with arbitrary paraxial illumination.

$$V_n(x, y) = A_n \exp(jkL_n)\exp\{jk[g_n(x - x_n)$$
$$+ h_n(y - y_n)]\}, \qquad (2)$$

where $A_n = A(x_n, y_n)$, $L_n = L(x_n, y_n)$, $g_n = (\partial L/\partial x)|_{x_n, y_n}$, and $h_n = (\partial L/\partial y)|_{x_n, y_n}$. When $g_n = h_n = 0$, the local plane wave is the normal illumination; in all the other cases, the local plane wave is the paraxially oblique illumination. It is well-known that a similar treatment has been used in the famous Shack–Hartmann wave-front sensors.[4] Substituting the approximation of the local plane wave into Eq. (1) and using the coordinate transforms $X' = X - x_n$, $Y' = Y - y_n$, $x' = x - x_n$, $y' = y - y_n$, $R' = \sqrt{X'^2 + Y'^2}$, and $r' = \sqrt{x'^2 + y'^2}$, one can obtain

$U_n(X, Y)$

$$= \frac{A_n}{\lambda q}\exp\left[jk\left(L_n + \frac{R'^2}{2q}\right)\right]$$

$$\times \int\int_{S_n}\exp\left(jk\frac{r'^2 - 2X''x' - 2Y''y'}{2q}\right)dx'dy', \qquad (3)$$

where $X'' = X' - g_n q$, $Y'' = Y' - h_n q$, and the integral area $S_n$ is $x'^2 + y'^2 \leq a_n^2$. By transforming the variables $x'$, $y'$, $X''$, and $Y''$ in the integral of Eq. (3) into the corresponding polar coordinate variables, we further express the field distribution $U_n(X, Y)$ as the following form (see Appendix A):

$$U_n(X, Y) = 2A_n \exp\left[jk\left(L_n + \frac{R'^2}{2q}\right)\right]F(\rho), \qquad (4)$$

$$F(\rho) = \frac{\pi}{\lambda q}\int_0^{a_n}\exp\left(jk\frac{r'^2}{2q}\right)J_0\left(\frac{k\rho}{q}r'\right)r'dr', \qquad (5)$$

where $\rho = \sqrt{X''^2 + Y''^2}$. One may note that, except for a phase factor, Eq. (5) has the same form as that of the Fresnel diffraction of a circular aperture illuminated by a uniform plane wave. However, one should keep in mind that the variable $\rho$ in Eq. (5) does not express the polar coordinate $(X^2 + Y^2)^{1/2}$, whose origin is located at the point $(X = 0, Y = 0)$, but rather expresses the polar coordinate $(X''^2 + Y''^2)^{1/2}$, whose origin is located at the point $(X = x_n + g_n q, Y = y_n + h_n q)$. In other words, $F(\rho)$ is a rotationally symmetric function about the point $(X = x_n + g_n q, Y = y_n + h_n q)$, but it is not a rotationally symmetric function about the coordinate origin $(X = 0, Y = 0)$. This shift comes about for two reasons: One is the location of the center of the pinhole, which shifts the symmetric center from $(X = 0, Y = 0)$ to $(X = x_n, Y = y_n)$; the other is the paraxially oblique illumination of the local plane wave at the pinhole area, which further shifts the symmetric center to $(X = x_n + g_n q, Y = y_n + h_n q)$.

Let us now investigate the asymptotic behavior of $F(\rho)$ when $q$ is large. Employing the moment expansion method,[5] one can expand the factor $\exp[jkr'^2/(2q)]$ as $\exp[jkr'^2/(2q)] \approx 1 + jkr'^2/(2q)$. Putting this approximation into Eq. (5), we get the first two terms $F_0(\rho)$ and $jF_1(\rho)$ (see Appendix B):

$$F_0(\rho) = N_f Jinc\left(\frac{ka_n}{q}\rho\right), \qquad (6)$$

$$F_1(\rho) = \frac{N_f^2}{12}\left[3J_0\left(\frac{ka_n}{q}\rho\right) + 2J_2\left(\frac{ka_n}{q}\rho\right) - J_4\left(\frac{ka_n}{q}\rho\right)\right], \qquad (7)$$

where $Jinc(\cdot) = J_1(\cdot)/(\cdot)$, $J_n(\cdot)$ is the $n$th-order Bessel function, and $N_f = \pi a_n^2/(\lambda q)$ is the Fresnel number. One can immediately find that $F_0(\rho)$ is nothing but the farfield (i.e., Fraunhofer diffraction) of the $n$th pinhole. The term $jF_1(\rho)$, as we shall investigate in Section 3, is the quasi-far-field correction term.

If the pinhole is small enough (concretely, the Fresnel number $N_f$ is smaller than 0.05), then, as we shall show in Section 3, the term $jF_1(\rho)$ is negligible. In this case, the first term $F_0(\rho)$ is good enough for describing the exact integral $F(\rho)$. We refer this approximation to the individual far-field model. Substituting the approximation $F(\rho) = F_0(\rho)$ into Eq. (4), one can obtain

$$U_n(X, Y) = 2N_f A_n \exp\left[jk\left(L_n + \frac{R'^2}{2q}\right)\right]Jinc\left(\frac{ka_n}{q}\rho\right). \qquad (8)$$

Equation (8) is the individual diffracted field of the $n$th pinhole. Accordingly, the total diffracted field distribution $U(X, Y)$ at the focal plane is the simple sum of those individual diffracted fields, i.e., $U(X, Y) = \Sigma_{n=1}^N U_n(X, Y)$. It is necessary to point out that the total diffracted field $U(X, Y)$ is not in the far-field (Fraunhofer diffraction) region but is still in the Fresnel diffraction region, although those individual diffracted fields are already in the far-field region. It is worth mentioning that a similar idea was recently used to distinguish between Fraunhofer diffraction and Fresnel diffraction.[6] In the work of Ref. 6, the individual diffracted fields of the two pinholes of Young's experiment are always in the far-field region because the pinholes are very small; however, the total diffracted field may be in the Fresnel diffraction region if the distance between the aperture and the observation plane is not far enough.

Let us now focus on the field value at the desired focal point $(X = 0, Y = 0)$. The crucial idea of the photon sieve is that all those individual diffracted fields from different pinholes have the same phase value (rigorously speaking, the same argument) or have a phase difference of $2m\pi$ at the desired focal point, where $m$ is an integer. This kind of collective behavior can greatly enhance the

intensity at the focal point and lead to focusing. From Eq. (8), one can immediately obtain $U_n(0, 0)$ at the point $(X = 0, Y = 0)$:

$$U_n(0, 0) = 2N_f A_n \exp\left[jk\left(L_n + \frac{r_n^2}{2q}\right)\right] J\mathrm{inc}\left(\frac{ka_n}{q}R_n\right),$$
(9)

where $r_n^2 = x_n^2 + y_n^2$ and $R_n = [(x_n + g_nq)^2 + (y_n + h_nq)^2]^{1/2}$. For simplicity, we choose the common phase (argument) value as $2m\pi$ (certain other values are also available). That is to say, $\arg[U_n(0, 0)] = 2m\pi$, where $\arg(\cdot)$ expresses the argument. The argument of the real function $J\mathrm{inc}(ka_nR_n/q)$ can be 0 or $\pi$, because this real function can be positive or negative. Correspondingly, the phase $k[L_n + r_n^2/(2q)]$ can be $2m\pi$ or $(2m + 1)\pi$. Therefore the selection condition can be briefly stated as follows:

$$k\left(L_n + \frac{r_n^2}{2q}\right) = 2m\pi, \qquad J\mathrm{inc}\left(\frac{ka_n}{q}R_n\right) > 0,$$
(10)

$$k\left(L_n + \frac{r_n^2}{2q}\right) = (2m + 1)\pi, \qquad J\mathrm{inc}\left(\frac{ka_n}{q}R_n\right) < 0.$$
(11)

Equations (10) and (11) are both valid for choosing the central positions and the radii of those pinholes. They are applicable to arbitrary paraxial illumination, because we do not use any specific requirement for the complex amplitude distribution $V(x, y)$ of the illuminative beam in the derivation. Of course, when the photon sieve is illuminated by a spherical wave of a point source, Eqs. (10) and (11) correspond to the cases of the white zones and the black zones used in Ref. 3, respectively. The first relation in Eq. (10) [or Eq. (11)] is used to determine the central positions $r_n$ of those pinholes, and the second relation in Eq. (10) [or Eq. (11)] is then used to further determine the radii $a_n$ of those pinholes. When Eq. (10) is used, $U_n(0, 0) = 2N_f A_n J\mathrm{inc}(ka_nR_n/q)$ because of the relation $\exp(j2m\pi) = 1$; and when Eq. (11) is used, $U_n(0, 0) = -2N_f A_n J\mathrm{inc}(ka_nR_n/q)$ because of the relation $\exp[j(2m + 1)\pi] = -1$. In both cases, $U_n(0, 0)$ has a simple relation with the function $J\mathrm{inc}(ka_nR_n/q)$. It is necessary to point out that, in the derivation of Eqs. (10) and (11), we have ignored the influence of the sign change of the real amplitude distribution $A(x, y)$. In other words, we have assumed that the real amplitude distribution $A(x, y)$ has the same sign over the whole photon sieve plane. This is not always the case. For example, the real amplitude distribution $A(x, y)$ will change its sign if a high-order Gaussian beam is used as the illuminative beam. However, if there is a sign change in $A(x, y)$, we can simply transform the negative sign into $\exp(j\pi)$ and put this $\pi$ phase into the first relations of Eqs. (10) and (11). Briefly speaking, in those regions where $A(x, y) > 0$, we use Eqs. (10) and (11); and in those regions where $A(x, y) < 0$ (if any exist), we exchange the first relations of Eqs. (10) and (11).

To understand the above statements better and have an intuitive impression, let us investigate the special case of spherical wave illumination of a point source. In this case, the eikonal is given by $L(x, y) = (x^2 + y^2)/(2p)$,

where $p$ is the distance between the point source and the photon sieve. Note that the paraxial approximation $x^2 + y^2 \ll p^2$ has been used and that the common constant $p$ has been ignored in this eikonal expression. From this expression, one can derive that $L_n = r_n^2/(2p)$, $g_n = x_n/p$, and $h_n = y_n/p$. Substituting these relations into Eq. (9), one can get

$$U_n(0, 0) = 2N_f A_n \exp\left[jk\left(\frac{r_n^2}{2f}\right)\right] J\mathrm{inc}\left(\frac{ka_n}{f}r_n\right), \quad (12)$$

where $f^{-1} = p^{-1} + q^{-1}$. It is interesting that the relation among $f$, $p$, and $q$ has the same form as that of the imaging formula of a thin lens. If the center of the pinhole is located at the center of a white zone, then the relation $\exp[jkr_n^2/(2f)] = 1$ holds. In this case, the contribution to the focusing from the $n$th pinhole is simply proportional to $a_n^2 J\mathrm{inc}(ka_nr_n/f)$. When $J\mathrm{inc}(ka_nr_n/f) > 0$, the pinhole has a positive contribution to the focusing; when $J\mathrm{inc}(ka_nr_n/f) < 0$, the pinhole has a negative contribution to the focusing. The changes from a positive (negative) contribution to a negative (positive) contribution happen when $J\mathrm{inc}(ka_nr_n/f) = 0$. From the property of the first-order Bessel function, one knows that these zeros appear at[7]

$$\frac{ka_nr_n}{f} = 3.832, 7.016, 10.173, 13.324,\dots. \quad (13)$$

On the other hand, according to the definition of a Fresnel zone, we know that the difference between the optical path length $\sqrt{r_n^2 + p^2} + \sqrt{r_n^2 + q^2}$ from the point source through the center of a white zone to the focal point and the optical path length $p + q$ from the point source directly to the focal point is an integral number of wavelengths. That is to say, $\sqrt{r_n^2 + p^2} + \sqrt{r_n^2 + q^2} - (p + q) = m\lambda$. In the paraxial approximations $p \gg r_n$ and $q \gg r_n$, this condition reduces to $r_n^2/(2f) = m\lambda$, which is completely equivalent to the relation $\exp[jkr_n^2/(2f)] = 1$ used above. Similarly, we know that the difference between the optical path length $[(r_n + w/2)^2 + p^2]^{1/2} + [(r_n + w/2)^2 + q^2]^{1/2}$ from the point source through the upper edge of a white zone to the focal point and the optical path length $[(r_n - w/2)^2 + p^2]^{1/2} + [(r_n - w/2)^2 + q^2]^{1/2}$ from the point source through the lower edge of the same white zone to the focal point is half a wavelength. That is to say, $[(r_n + w/2)^2 + p^2]^{1/2} + [(r_n + w/2)^2 + q^2]^{1/2} - [(r_n - w/2)^2 + p^2]^{1/2} - [(r_n - w/2)^2 + q^2]^{1/2} = \lambda/2$. In the paraxial approximations $p \gg r_n + w/2$, $p \gg r_n - w/2$, $q \gg r_n + w/2$, and $q \gg r_n - w/2$, one can prove that this relation reduces to

$$\frac{kr_n}{f} = \frac{\pi}{w}. \quad (14)$$

Substituting Eq. (14) into Eq. (13), one can immediately obtain that those changes occur when

$$\frac{d}{w} = 2.44, 4.47, 6.48, 8.48,\dots, \quad (15)$$

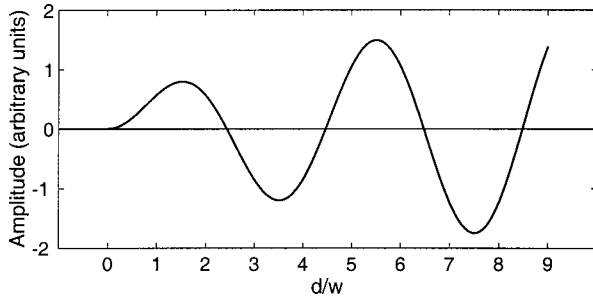where $d = 2a_n$ is the diameter of the pinhole. Obviously, these results are in excellent agreement with those

Fig. 2. Analytical description of the detailed change of the field value $U_n(0, 0)$ at the focal point with the increase of the ratio $d/w$. The center of the pinhole is located at the center of a white zone.

$d/w$ values of approximately 2.4, 4.4, 6.4,... that were obtained by the numerical calculation of Fresnel–Kirchhoff diffraction integrals in Ref. 3. We further investigate the detailed change of the field value $U_n(0, 0)$ with the increase of the ratio $d/w$. Substituting Eq. (14) into Eq. (12), one can obtain the following for a pinhole whose center is located at the center of a white zone:

$$U_n(0, 0) \propto \frac{d}{w} J_1\left(\frac{\pi}{2} \frac{d}{w}\right). \quad (16)$$

The functional relation of expression (16) is shown in Fig. 2. Simply comparing this figure with the curve labeled "Total" in Fig. 2 of Ref. 3, one can find that they are in excellent agreement. In particular, besides the positions of those zeros investigated above, Fig. 2 also clearly shows that, just as found from the numerical calculation of Fresnel–Kirchhoff diffraction integrals,[3] those maximum values of $|U_n(0, 0)|$ appear when $d/w \approx 1.5, 3.5, 5.5, 7.5$, and so on.

## 3. INDIVIDUAL QUASI-FAR-FIELD CORRECTION FOR VERY LARGE PINHOLES

Let us now check the validity range of the individual far-field model and discuss the individual quasi-far-field corrections for very large pinholes. These investigations can be implemented by comparing the formulas $F_0(\rho)$ and $jF_1(\rho)$ with the exact integral $F(\rho)$. It is appropriate to employ the normalized coordinates $\rho_1 = r'/a_n$ and $\rho_2 = \rho/a_n$. In terms of these new parameters, Eqs. (5)–(7) can be reexpressed as

$$F(\rho_2) = N_f \int_0^1 \exp(jN_f\rho_1^2)J_0(2N_f\rho_1\rho_2)\rho_1 d\rho_1, \quad (17)$$

$$F_0(\rho_2) = N_f J\text{inc}(2N_f\rho_2), \quad (18)$$

$$F_1(\rho_2) = \frac{N_f^2}{12}[3J_0(2N_f\rho_2) + 2J_2(2N_f\rho_2)$$

$$- J_4(2N_f\rho_2)]. \quad (19)$$

We find that, as shown in Fig. 3, the far-field term $F_0(\rho_2)$ is highly accurate for the exact integral $F(\rho_2)$ when the Fresnel number $N_f$ is smaller than 0.05. When $N_f$ increases, the difference between $F(\rho_2)$ and $F_0(\rho_2)$ also increases. However, as shown in Fig. 4, the sum $F_0(\rho_2) + jF_2(\rho_2)$ is still highly accurate even when $N_f$
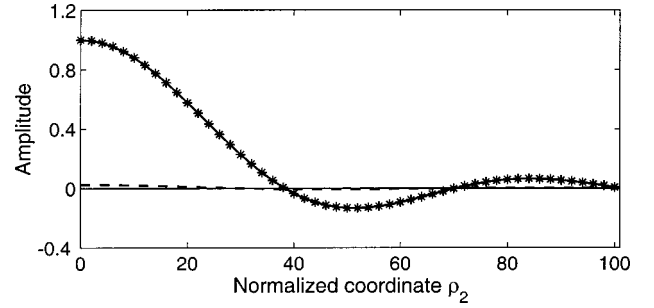


Fig. 3. Comparison between the individual far-field term $F_0(\rho_2)$ and the exact numerical integral $F(\rho_2)$. The solid line is the real part of $F(\rho_2)$, and the asterisks are the far-field term $F_0(\rho_2)$. The Fresnel number $N_f$ is chosen such that $N_f = 0.05$. The field values have been normalized according to $F_0(\rho_2 = 0) = 1$. The negligible imaginary part of the exact numerical integral $F(\rho_2)$ is also shown as the dashed curve.
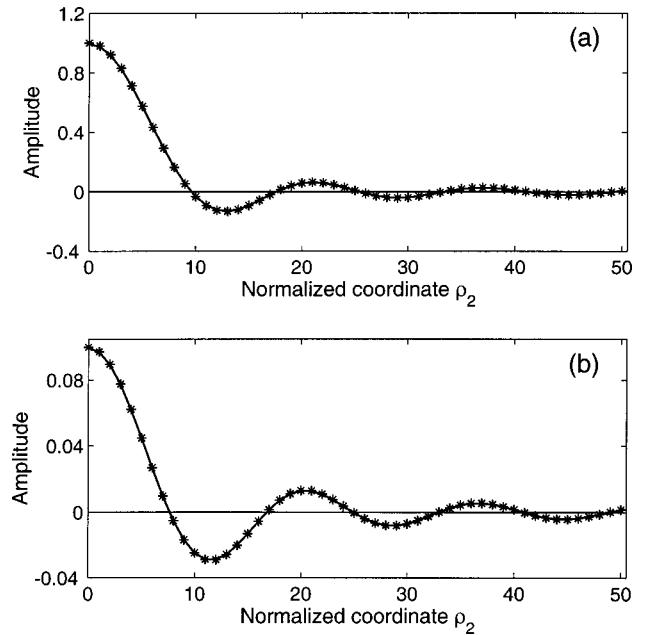


Fig. 4. Comparison between the individual quasi-far-field approximation [i.e., the sum of the far-field term $F_0(\rho_2)$ and the quasi-far-field correction term $jF_1(\rho_2)$] and the exact numerical integral $F(\rho_2)$. The Fresnel number $N_f$ is chosen such that $N_f = 0.2$. The field values have been normalized according to $F_0(\rho_2 = 0) = 1$. (a) The solid line is the real part of $F(\rho_2)$, and the asterisks are the far-field term $F_0(\rho_2)$. (b) The solid line is the imaginary part of $F(\rho_2)$, and the asterisks are the quasi-far-field correction term $F_1(\rho_2)$.

= 0.2. To have an intuitive understanding of these results, let us visit the optical prototype of the photon sieve of Ref. 3, where the wavelength $\lambda$ and the focal length $q$ are chosen such that $\lambda = 0.6328 \mu$m and $q = 1$ m. In this optical prototype, the value 0.05 of the Fresnel number $N_f$ corresponds to a diameter of approximately 200 $\mu$m of a large pinhole, and the value 0.2 of the Fresnel number $N_f$ corresponds to a diameter of approximately 400 $\mu$m of a very large pinhole. From the zoomed photon sieve figure and the sentence "The diameter of the photon sieve is 10 mm" of the online article "Pinholes produce sharp focus" in the site http://optics.org/article/news/7/11/

21, we deduced that the diameter of the largest pinholes used in this photon sieve is approximately 200 $\mu$m. The corresponding Fresnel number is approximately 0.05. These results show that the individual far-field model is good enough for the focusing analysis of photon sieves, at least for that of the above-mentioned optical prototype. It is worth mentioning that we do not intend to use the value $N_f = 0.05$ as a criterion for distinguishing between Fresnel and Fraunhofer diffractions. Generally speaking, it is difficult to give a general criterion to distinguish between these two kinds of diffractions because different applications may require different accuracies. Reference 6 reasonably proposed a criterion of $N_f = 0.2232\pi$ (note that the definition of Fresnel number used here is $\pi$ times that used there) from the overall character. We here use a stricter value of $N_f = 0.05$ because we want to keep higher accuracy. Extremely high accuracy is necessary here because the final field distribution at the focal plane is the sum of many individual diffracted fields from different pinholes. Low accuracy in individual diffracted fields may lead to large error in the total diffracted field.

It is necessary to point out that the above two checks are not only valid for the field value at the desired focal point but also valid for the field distribution well off the optical axis. We mean that the two checks are valid for the field distribution at the whole focal plane. To understand this statement better, let us visit Figs. 3 and 4 and the optical prototype of the photon sieve again. As said above, in the optical prototype, the values 0.05 and 0.2 of the Fresnel number $N_f$ correspond to radii of 100 and 200 $\mu$m for the pinhole, respectively. Consequently, the range $0 \leqslant \rho_2 \leqslant 100$ in Fig. 3 and the range $0 \leqslant \rho_2 \leqslant 50$ in Fig. 4 correspond to the same range $0 \leqslant \rho \leqslant 10$ mm in the focal plane. Therefore Figs. 3 and 4 directly check the validity of the far-field model and the quasi-far-field correction for the region $0 \leqslant \rho \leqslant 10$ mm in the focal plane. If we choose the central position of the pinhole as $r_n = 5$ mm (i.e., at the edge of the photon sieve, which is the worst case), then, from the values of $p = 20$ m and $q = 1$ m of the optical prototype,[3] one can find that the central position of the diffracted field shifts to $\sqrt{X^2 + Y^2}$ = 5.25 mm at the focal plane. Then one can further deduce that the circular region $0 \leqslant \sqrt{X^2 + Y^2} \leqslant 4.75$ mm, which is large enough for any practical interest, is always completely covered by the range $0 \leqslant \rho \leqslant 10$ mm. This confirms the statement at the beginning of this paragraph. As a consequence, the total field distribution and the total intensity distribution at the focal plane can also be accurately described by the far-field model and the quasi-far-field correction through linear superposition of those individual diffracted fields.

For completeness, let us now discuss the individual quasi-far-field correction term $jF_1(\rho)$ and some related problems for very large pinholes. From Eqs. (6) and (7), one can find that $F_0(\rho)$ is purely real and $jF_1(\rho)$ is purely imaginary. As a consequence, these two terms are "incoherent" because of the relation $|F_0(\rho) + jF_1(\rho)|^2 = |F_0(\rho)|^2 + |F_1(\rho)|^2$. As we stated in Section 2, the argument of $F_0(\rho)$ is either 0 or $\pi$, because $F_0(\rho)$ is purely real. However, if the term $jF_1(\rho)$ is not negligible, the argument $\varphi(\rho)$ for the sum $F_0(\rho) + jF_1(\rho)$ is no longer 0

or $\pi$, because the quasi-far-field correction term $jF_1(\rho)$ is not real. This change in the argument $\varphi(\rho)$ in turn slightly changes the selection conditions of Eqs. (10) and (11) for the positions and the radii of those pinholes. The generalized form of Eqs. (10) and (11) can be briefly written as

$$k\left(L_n + \frac{r_n^2}{2q}\right) + \varphi(R_n) = 2m\pi, \qquad (20)$$

where $\varphi(R_n)$ is the argument of $F_0(R_n) + jF_1(R_n)$, which is the individual field value at the desired focal point. One can prove that Eq. (20) reduces to Eqs. (10) and (11) in the approximation $F_1(R_n) = 0$. Concretely, when $F_1(R_n) = 0$ and $F_0(R_n) > 0$, one can obtain Eq. (10) by taking the relation $\varphi(R_n) = 0$ into account; when $F_1(R_n) = 0$ and $F_0(R_n) < 0$, one can obtain Eq. (11) by taking the relation $\varphi(R_n) = \pi$ into account. We call the change of the argument $\varphi(R_n)$ from 0 or $\pi$ the phase shift induced by the individual quasi-far-field correction. We emphasize that this induced phase shift is necessary only for very large pinholes (i.e., the Fresnel number is larger than 0.05). For those pinholes whose Fresnel number is smaller than 0.05, there is no need to employ Eq. (20). In this case, Eqs. (10) and (11) are good enough.

## 4. CONCLUSIONS AND DISCUSSIONS

We have presented the individual far-field model for the focusing analysis of general photon sieves illuminated by an arbitrary paraxial beam with arbitrary complex amplitude distributions. This simple analytical model has been demonstrated to be accurate by comparing it with the corresponding exact numerical integral. Based on this model, the selection conditions for the positions and the radii of those pinholes are given by Eqs. (10) and (11). As an example, we have shown that, for the special case of spherical wave illumination of a point source, the results given by our model are in excellent agreement with those obtained from numerical calculation of Fresnel–Kirchhoff diffraction integrals in Ref. 3. We also analytically presented the quasi-far-field correction term and showed that this term is needed only for very large pinholes (the Fresnel number is larger than 0.05). For very large pinholes, the phase shift induced by the quasi-far-field correction term should be taken into account. In this case, one should use the generalized selection condition of Eq. (20) to replace Eqs. (10) and (11).

In addition, the analytical expressions for the individual far-field and individual quasi-far-field correction terms can be directly used for the fast and highly accurate simulation of pinhole photon sieves (after the positions and the radii of those pinholes have been determined). Simply replacing the integral $F(\rho)$ in Eq. (4) by the sum $F_0(\rho) + jF_1(\rho)$, whose terms are given in Eqs. (6) and (7), one can obtain the individual diffracted field $U_n(X, Y)$ from the $n$th pinhole. One trivial point in this step is that one can use the expression $F_0(\rho) = N_f[J_0(ka_n\rho/q) + J_2(ka_n\rho/q)]/2$ to calculate the far-field term $F_0(\rho)$ because of the relation[7] $J_1(\cdot)/(\cdot) = [J_0(\cdot) + J_2(\cdot)]/2$. This treatment can avoid the case of 0/0 (i.e., zero divided by zero) when $\rho = 0$ in the numerical calculation. Then,

by simply calculating the sum of all those individual diffracted fields, i.e., implementing $U(X, Y) = \Sigma_{n=1}^{N} U_n(X, Y)$, one can obtain the total field distribution $U(X, Y)$ at the focal plane. And then the simulated intensity distribution $I(X, Y)$ can be easily determined by the relation $I(X, Y) = |U(X, Y)|^2$. This simulation method is much faster than that[3] based on the direct numerical calculation of Fresnel–Kirchhoff diffraction integrals of those pinholes, because the analytical expressions are employed in the calculation of those individual diffracted fields.

The analyses in this paper are based on the following approximations. The first one is the paraxial approximation, or equivalently the Fresnel diffraction integral. This approximation is widely used and is satisfactory in almost all cases. For example, for the optical prototype of the photon sieve, the distance $p$ between the point source and the photon sieve plane is 20 m, and the radius of the photon sieve is 5 mm. From these two data, one can deduce that the divergence angle of the illumination beam at the photon sieve area is less than 0.25 mrad. Therefore the paraxial approximation is well satisfied in this case. The second one is the local plane-wave approximation for the fields inside those pinholes. This approximation is always satisfied because the pinholes are very small compared with the range over which the complex amplitude distribution of the illuminative beam has a significant change. The third one and the fourth one are the far-field and quasi-far-field approximations for the diffracted fields of individual pinholes, respectively. As we have shown above, the individual far-field model accurately holds when the corresponding Fresnel number $N_f$ is smaller than 0.05, and the quasi-far-field approximation accurately holds when the corresponding Fresnel number $N_f$ is smaller than 0.2. The high degree of validity of these approximations for a photon sieve structure ensures that the results obtained in this paper are robust and reliable.

## APPENDIX A

Employing the polar coordinate variables $\rho$, $\phi$, $r'$, and $\theta$ through the transforms $X'' = \rho \cos \phi$, $Y'' = \rho \sin \phi$, $x' = r' \cos \theta$, $y' = r' \sin \theta$, and $\mathrm{d}x'\mathrm{d}y' = r'\mathrm{d}r'\mathrm{d}\theta$, one can express the integral in Eq. (3) as

$$\int_0^{a_n} \exp\left(jk\frac{r'^2}{2q}\right) C(\rho, r') r' \mathrm{d}r', \qquad (A1)$$

where

$$C(\rho, r') = \int_0^{2\pi} \exp\left(-jk\rho r' \frac{\cos \phi \cos \theta + \sin \phi \sin \theta}{q}\right) \mathrm{d}\theta. \qquad (A2)$$

Because the system considered here is circularly symmetric about $\rho$ and $r'$, the function $C(\rho, r')$ must be independent of the angle $\phi$. For simplicity, we let $\phi = 0$. In this case, $C(\rho, r')$ can be more simply written as

$$C(\rho, r') = \int_0^{2\pi} \exp\left(-j\frac{k\rho r'}{q}\cos \theta\right) \mathrm{d}\theta. \qquad (A3)$$

Employing the equality[7]

$$J_0(-v) = \frac{1}{2\pi} \int_0^{2\pi} \exp(-jv \cos \theta) \mathrm{d}\theta$$

and the property $J_0(-v) = J_0(v)$, where $v = k\rho r'/q$, one can further obtain

$$C(\rho, r') = 2\pi J_0\left(\frac{k\rho}{q}r'\right). \qquad (A4)$$

Substituting Eq. (A4) into the integral (A1), and then substituting into Eq. (3), one can immediately obtain Eqs. (4) and (5).

## APPENDIX B

Putting the approximation[5] $\exp[jkr'^2/(2q)] = 1 + jkr'^2/(2q)$ into Eq. (5), one can express $F(\rho)$ as $F(\rho) = F_0(\rho) + jF_1(\rho)$, where $F_0(\rho)$ and $F_1(\rho)$ are given by

$$F_0(\rho) = \frac{\pi}{\lambda q} \int_0^{a_n} J_0\left(\frac{k\rho}{q}r'\right) r' \mathrm{d}r', \qquad (B1)$$

$$F_1(\rho) = \frac{\pi}{\lambda q} \int_0^{a_n} \frac{kr'^2}{2q} J_0\left(\frac{k\rho}{q}r'\right) r' \mathrm{d}r'. \qquad (B2)$$

Equations (B1) and (B2) can be further expressed as the following forms:

$$F_0(\rho) = \frac{N_f}{u^2} \int_0^u v J_0(v) \mathrm{d}v, \qquad (B3)$$

$$F_1(\rho) = \frac{N_f^2}{u^4} \int_0^u v^3 J_0(v) \mathrm{d}v, \qquad (B4)$$

where $u = k\rho a_n/q$ and $v = k\rho r'/q$. Substituting the equality[7] $\int_0^u v J_0(v)\mathrm{d}v = u J_1(u)$ into Eq. (B3), one can obtain

$$F_0(\rho) = N_f \frac{J_1(u)}{u}, \qquad (B5)$$

which is just Eq. (6).

Substituting the equality $\int_0^u v^3 J_0(v)\mathrm{d}v = 2u^2 J_0(u) + (u^3 - 4u)J_1(u)$ into Eq. (B4), one can obtain

$$F_1(\rho) = \frac{N_f^2}{u^2}\left[2J_0(u) + uJ_1(u) - 4\frac{J_1(u)}{u}\right]. \qquad (B6)$$

Substituting the equality[7] $J_1(u)/u = [J_0(u) + J_2(u)]/2$ into Eq. (B6), one can further obtain

$$F_1(\rho) = N_f^2\left[\frac{J_1(u)}{u} - \frac{2}{u}\frac{J_2(u)}{u}\right]. \qquad (B7)$$

Further employing the relation[7] $J_n(u)/u = [J_{n+1}(u) + J_{n-1}(u)]/(2n)$, one can obtain

$$F_1(\rho) = \frac{N_f^2}{2}\left[J_0(u) + J_2(u) - \frac{J_1(u)}{u} - \frac{J_3(u)}{u}\right]. \qquad (B8)$$

One can prove that Eq. (B8) is just Eq. (7) after using the equality $J_n(u)/u = [J_{n+1}(u) + J_{n-1}(u)]/(2n)$ again.

## ACKNOWLEDGMENT

The authors are indebted to Stefan Sinzinger for many fruitful discussions.

## REFERENCES

1.  G. Schmahl, D. Rudolph, P. Guttmann, and O. Christ, "Zone plates for x-ray microscopy," in *X-Ray Microscopy*, G. Schmahl and D. Rudolph, eds. (Springer-Verlag, Berlin, 1984), Vol. 43, pp. 63–74.
2.  E. H. Anderson, V. Boegli, and L. P. Muray, "Electron beam lithography digital pattern generator and electronics for generalized curvilinear structures," J. Vac. Sci. Technol. B **13**, 2529–2534 (1995).
3.  L. Kipp, M. Skibowski, R. L. Johnson, R. Berndt, R. Adelung, S. Harm, and R. Seemann, "Sharper images by focusing soft x-rays with photon sieve," Nature (London) **414**, 184–188 (2001).
4.  See, for example, R. K. Tyson, *Principles of Adaptive Optics*, 2nd ed. (Academic, Boston, Mass., 1998), Subsect. 5.3.2.
5.  Y-T. Wang, Y. C. Pati, and T. Kailath, "Depth of focus and the moment expansion," Opt. Lett. **20**, 1841–1843 (1995).
6.  J. I. García-Sucerquia, R. Castañeda, F. F. Medina, and G. Matteucci, "Distinguishing between Fraunhofer and Fresnel diffraction by the Young's experiment," Opt. Commun. **200**, 15–22 (2001).
7.  M. Abramowitz and I. A. Stegun, eds., *Handbook of Mathematical Functions with Formulas, Graphs, and Mathematical Tables* (Wiley, New York, 1972).